Scripta Materialia 172 (2019) 1–5

Contents lists available at ScienceDirect

Scripta Materialia

journal homepage: www.elsevier.com/locate/scriptamat

Flash sintering of Li-ion conducting ceramic in a few seconds at 850 °C

Thomas Clemenceau [a], Niriaina Andriamady [a,*], Punith Kumar M.K. [a], Aly Badran [a], Viviana Avila [a], Keith Dahl [b], Mira Hopkins [b], Xavier Vendrell [c], David Marshall [a], Rishi Raj [a]

[a] Department of Mechanical Engineering, University of Colorado at Boulder, Boulder, CO 80309, USA
[b] American Manufacturing, Inc., 685 S Arthur Ave, Unit 7A, Louisville, CO 80027, USA
[c] Department of Materials Science, Sheffield University, Sheffield, UK

ARTICLE INFO

Article history:
Received 29 April 2019
Received in revised form 13 June 2019
Accepted 28 June 2019
Available online 10 July 2019

Keywords:
Lithium ion batteries
Solid state electrolyte
LLZO

ABSTRACT

Short sintering times and low furnace temperatures characterize the flash sintering process. The method can enable sintering of compounds of lithium since, in conventional sintering, which requires several hours at high furnace temperatures, it can become difficult to control the retention of lithium. Cubic $Li_{6.25}La_3Zr_2Al_{0.25}O_{12}$ with a relative density of 96% was sintered in a few seconds in air at a furnace temperature of 850 °C. These specimens had an ionic conductivity of 0.5 mS cm^{-1} at room temperature, and an activation energy of 0.35 eV. Transgranular nature of the fracture surface suggests strong cohesion at grain boundaries.

Flash sintering, first reported in 2010 [1,2], is a process whereby nearly full relative density can be achieved in mere seconds by applying an electric field to the specimen at furnace temperatures that are significantly below the temperatures needed in conventional sintering. It has been shown to apply to a broad class of oxides, including semiconductors (e.g. Co_2MnO_4), electronic conductors (e.g. TiO_2), ionic conductors (e.g. ZrO_2) and insulators (e.g. Y_2O_3) [3].

A typical experimental arrangement is shown in Fig. 1(a) and (b). The experiments in our laboratory are done with specimens in the shape of dog bones. These specimens are hung within a furnace with metal wires which also carry the electrical power directly to the specimen. The furnace temperature is controlled independently of the electrical circuit connected to the specimen. The "flash" is initiated under a combination of furnace temperature and electrical field; the field and temperature are inversely related, i.e., the flash temperature increases if the field is reduced. The temperature-field duo varies from one oxide to another. However, the phenomenological behavior is common to all oxides: flash is signaled by an abrupt increase in the electrical conductivity. The runaway current is controlled by switching the power supply from voltage to current control. The sample sinters to high relative density during this short period of transition from voltage to current control. Thus, sintering is achieved in a few seconds at low furnace temperatures. However, it is to be noted that the specimen heats up above the furnace temperature from the rise in the current at the onset of flash [4].

The results presented in this letter were obtained in the quest of sintering the cubic phase of LLZO-Al ($Li_{6.25}La_3Zr_2Al_{0.25}O_{12}$) quickly at low furnace temperatures to pre-empt the loss of lithium. Sintering requires solid-state chemical diffusion, which is controlled by the transport of the slowest moving species. Therefore, fast diffusion of Li^+ which renders it viable as a solid-state electrolyte at ambient temperature, becomes an impediment during sintering; lithium can migrate to the surface, react with air and volatilize as Li_2O.

Several experiments related to sintering of LLZO (without flash) have been reported since Murugan et al. [5] achieved a relative density of 92% by annealing pellets for 36 h in air at a temperature of 1230 °C. The heating rate for these experiments was 1 °C min^{-1}, which increased the sintering time to >50 h. Ionic conductivity of 0.77 mS cm^{-1} was achieved. Later efforts concentrated on reducing the sintering time and temperature for densification. Sudo et al. [6] could lower the sintering temperature to 1180 °C for a relative density of 89.6%. More recently Hu et al. [7] reported reducing the time to 12 h and the temperature to 1160 °C for a density of 87.7%. The cubic phase, instilled by doping with alumina, generally leads to higher density, e.g. to 93.7% [8,9].

Hot pressing within a graphite die in Ar atmosphere with a pressure of 40–62 MPa further reduced the sintering time and increased the relative density. For example, cubic LLZO(Al) was sintered in 1 h to a density of 96–99.4% [9–11]. Lower processing temperatures generally led to a lower density [12]. The ionic conductivity of these specimens generally ranged from 0.1 to 0.5 mS cm^{-1}, with the higher conductivities correlating with higher physical density.

We now describe the method and the results from flash sintering of cubic, Al_2O_3-doped LLZO, with commercially produced powders, in the apparatus illustrated in Fig. 1. The method consisted of pressing the

* Corresponding author.
E-mail address: Niriaina.Andriamady@gmail.com (N. Andriamady).

https://doi.org/10.1016/j.scriptamat.2019.06.038
1359-6462/

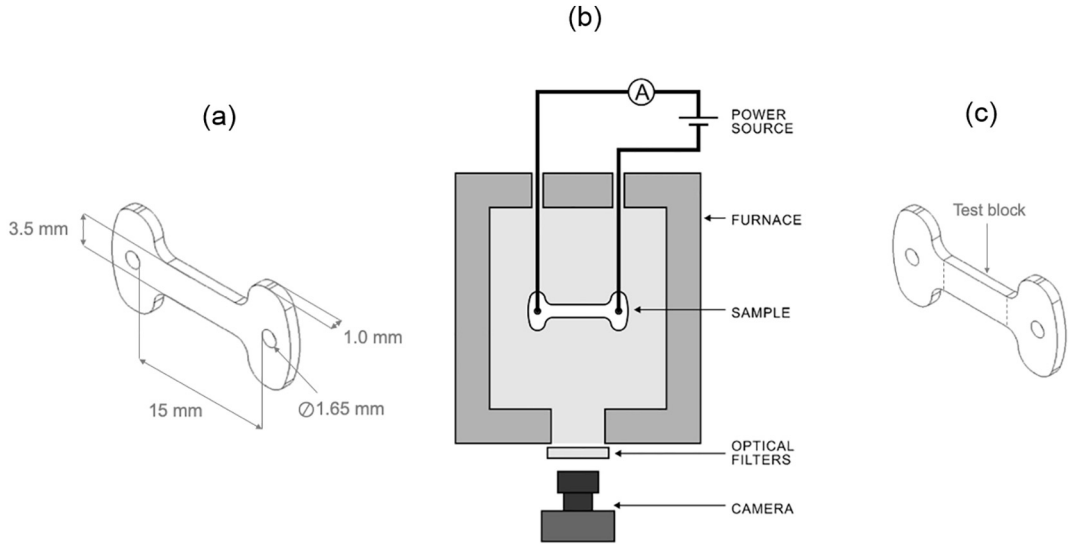

Fig. 1. (a) Geometry of the dog-bone specimen, (b) typical architecture of the flash sintering setup, and (c) cutting marks to obtain a rectangular block from a flash sintered dog-bone specimen for characterization.

ceramic powder into the shape of a dog bone with a typical gage length of 15 mm and a cross section of 3.5 mm × ~1.0 mm. The specimen was hung within a furnace held at a constant temperature with kanthal wires, and silver paste was applied to improve the contact. Electrical power was supplied to the specimen through these wires [1]. The experiment began with holding the furnace at a constant temperature and applying a constant electric field to the specimen as a step function. The onset of flash was signaled by a sudden increase in conductivity; thermal runaway was prevented by switching the power supply to current control. Sintering occurred during this switching event. The specimen was then held under current control for a few seconds and the power to the specimen and to the furnace was disconnected. The specimen was now ready for characterization.

The experiments were carried out with a commercial powder obtained from Toshima Manufacturing Co., Ltd., Saitama, JAPAN, with manufacturer specified particle size of 1 μm. The powder was pressed in a die to a green density of ~50%. The electrical field and current to the specimen were supplied by a KL series power supply obtained from Glassman, High Bridge, NJ. The power supply is capable of switching from voltage to current control within 50 ms. A CCD camera, the DMK Model from The Imaging Source, Charlotte, NC, recorded the change in the sample dimensions through a series of optical filters. The true linear shrinkage strain, ε, was measured from the optical images using the equation $\varepsilon = \ln(l/l_0)$, where l_0 is the initial gage length and l is the time-dependent gage length as the specimen sinters [1]. The final density, ρ, was calculated from the equation [13], $\rho = \rho_g e^{-3\varepsilon}$, where ρ_g is the green density. Software, built on the MATLAB platform has been developed to control the process, analyze the data, and translate the images into sintering strain, in real time.

The flash sintering experiments was performed with the furnace held at 850 °C. The specimen flashed almost immediately as signaled by a rise in the current. The power supply was programmed to switch to current control at the onset of this event with the current limit set to 190 mA mm^{-2}. These process parameters (furnace temperature, electrical field and the current limit) were optimized through several experiments in order to obtain a high density and a uniform microstructure across the gage section of the dog-bone. (According to Francis and Raj [14], the onset of flash depends on the furnace temperature and the field while the extent of densification is related to the current limit.)

The voltage profile (expressed in V cm^{-1}), the current flowing through the specimen (in mA mm^{-2}), and the power dissipation, given by the product of the field and the current density, are shown in Fig. 2(a). The zero point of the time scale refers to the application of the electric field. The current rose within 1 s to ~100 mA mm^{-2}, and then gradually increased to the current limit of 190 mA mm^{-2}, within ~8 s, while the field declined to ~20 V cm^{-1}. The power dissipation fluctuated between 320 and 570 mW mm^{-3}. The electrical current to the specimen was turned off at ~15 s. The time dependent true strain as a function of time is reported on the right-hand side in Fig. 2(b). The characteristic feature of flash sintering [1] is seen in the nearly vertical slope of the shrinkage curve as soon as the current limit is reached. There is no further shrinkage as the specimen is held at constant current for a few seconds before ending the experiment.

The specimen temperature rises during the flash with the current flowing through it. The temperature was measured with a pyrometer and is shown in Fig. 2(c) to rise to nearly 1300 °C for a few seconds during the flash. However, this very short period of high temperature exposure does not appear to harm the development of the dense microstructure or the electrochemical properties of the ceramic. Still, it is possible that some lithium was lost from the surface. This aspect of the sintering process needs to be further controlled and studied.

At the end of the experiment, the shrinkage strain was −0.22, which, using the equations given earlier in this letter, translates into a final relative density of 96.5% ± 1%. Physical measurement of the density from weight and volume of a rectangular section cut from the gage section, when compared with the theoretical density of cubic Al-LLZO, 5.107 g cm^{-3}, agreed with the relative density measured from the linear shrinkage, permitting the conclusion that shrinkage in the specimen was isotropic along the length and the transverse directions of the gage section of the specimen.

The flash sintered specimens were further characterized by scanning electron microscopy and by X-ray diffraction. These results are given in Fig. 3. Figure (a) shows the SEM micrograph of a fracture surface while figure (b) compares the X-ray diffraction pattern to the handbook data [15]. The SEM image is consistent with very low porosity in the specimen, expected from its high relative density. The fracture morphology is seen to be transgranular, which implies strong cohesion at grain boundaries, that can facilitate the transport of lithium ions across the grain boundaries [16]. The X-ray diffraction pattern is consistent with the pattern expected from the cubic phase of LLZO.

The hardness, H, and fracture toughness, K_{1C}, measured by the indentation method, were respectively ~6.4 GPa and ~1.1 MPa $m^{1/2}$, in good agreement with the literature values [16–18].

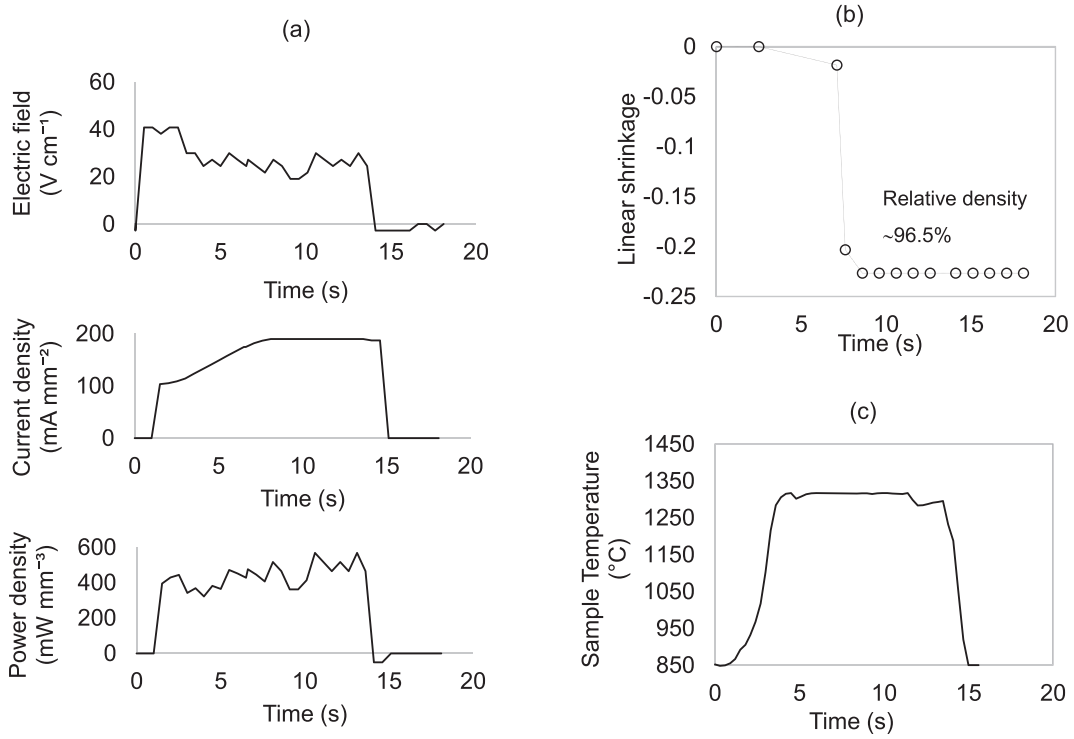

Fig. 2. (a) Electric field, current density, and power density curves, (b) linear shrinkage, and (c) specimen temperature during flash sintering of LLZO.

The ionic conductivity of the specimens was measured by impedance spectroscopy with 4192A LF impedance analyzer; HP, Palo Alto, CA, in the frequency range of 5 Hz to 10 MHz with a voltage amplitude at 0.1 V. Zview software, from Scribner Associates Inc., Southern Pines, NC, US, was used for data analysis and presentation of the impedance spectrum. An environmental chamber, ESPEC North America, Inc., Hudsonville, MI, was used to measure the temperature dependence of the ionic conductivity from 233 to 293 K.

The specimens for impedance measurements were prepared by cutting rectangular blocks from the gage section with dimensions of 4 × 3 × 0.9 mm as shown in Fig. 1(c). Half cells were assembled with lithium foil bonded to both surfaces of the specimen in an argon-filled glove box at <0.25 ppm of oxygen. Lithium foil, obtained from the MTI Corporation, CA, was cut to match the surface area of the LLZO specimen. The foils were then diffusion bonded to the surfaces of the electrolyte under a pressure of 8 MPa for 30 min at 150 °C. The symmetrical Li|LLZO|Li half-cell was placed inside Swagelok-type test cell for measurement of the electrochemical properties in air.

A typical impedance spectrum of the Li-LLZO-Li cells at room temperature is shown in Fig. 4(a). It consists of two distinct semicircles, which

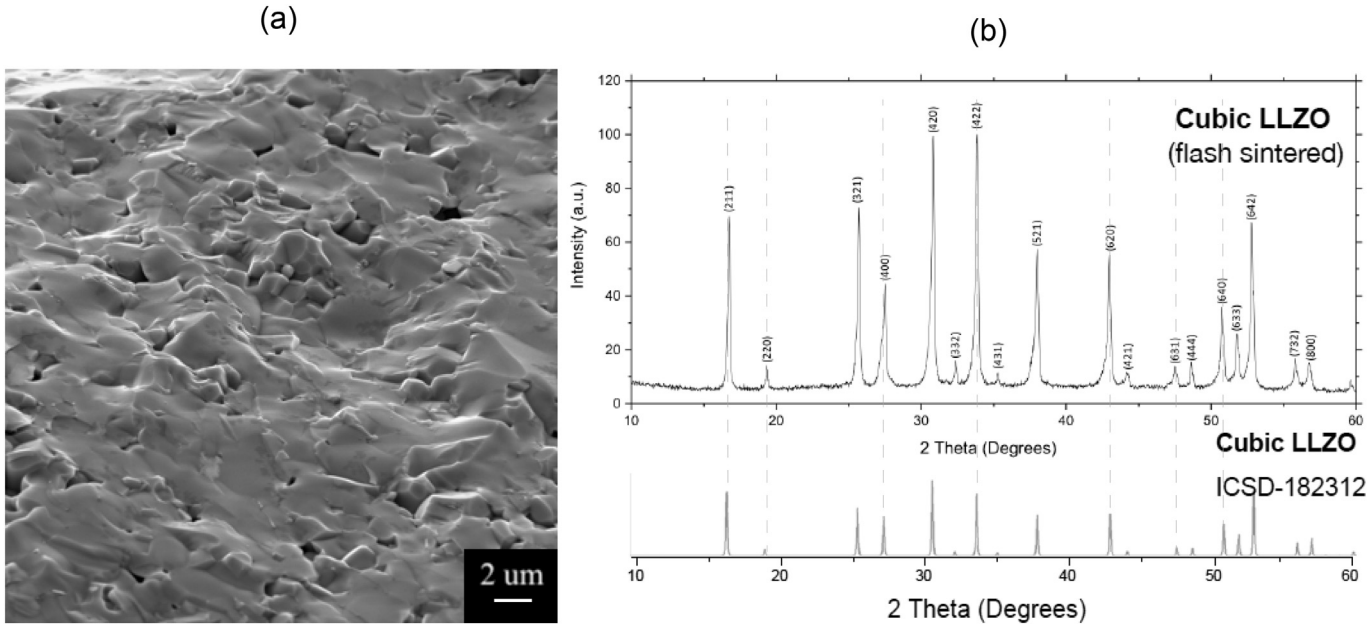

Fig. 3. (a) SEM image of flash sintered LLZO fracture surface, (b) XRD pattern of flash sintered LLZO; ICSD-182312 is a reference of cubic LLZO.

were interpreted to represent the LLZO electrolyte resistance at high frequency and the high Li-LLZO interfacial resistance at low frequency [19,20]. We were unable to resolve the high frequency semicircle into grain boundary and bulk resistance. Thus, we report here the total (grain boundary + bulk) resistance of the cubic LLZO as given by the intercept of the semicircle along the real (resistive) axis of the impedance plot [7,19–21]. In this way the ionic conductivity of the flash sintered electrolyte is measured to be 0.5 mS $cm^{-1} \pm 0.05$ mS cm^{-1}. Nearly forty flash sintered LLZO specimens prepared with the same method yielded consistent values for the room temperature ionic conductivity, expressed here in units of area specific resistance (ASR) in Ohms cm^2 in Fig. 4b, all lying within 10% of one another. This value is consistent with higher end of the literature values obtained from samples prepared by conventional sintering and hot-pressing techniques [5–7,9–12].

The activation energy for flash sintered LLZO was obtained from the measurement of the ionic conductivity at −40 °C, −20, 0, and 20 °C. The impedance data are shown in Fig. 4(c). An Arrhenius plot [7,21] for these data is given in Fig. 4(d). The plot yields an activation energy of 0.35 eV, which lies well within the range of values reported for LLZO and Al-doped LLZO of 0.28 to 0.54 eV [5,7,10,22].

The following equations were used to obtain the specific conductivity and the ASR values given in Fig. 4. The specific conductivity, $\sigma = \frac{L}{R.A}$ where σ (S cm^{-1}) is the conductivity, R is the resistance, L (cm) is the thickness of the ceramic specimen, and A (cm^2) is the area of symmetrical electrode. The activation energy was calculated from the Arrhenius equation: $\sigma T = Bexp(-\frac{E_a}{k_B T})$ where B is the pre-exponential factor, E_a (J $atom^{-1}$) is the activation energy, k_B is the Boltzmann constant, and T (K) is the absolute temperature. The ASR is given by $ASR = L/\sigma$ in Ω cm^{-2}.

This is most likely the first report of flash sintering of a Li-ion conducting ceramic electrolyte. It has been demonstrated that cubic-LLZO of high relative density, with reasonably ionic conductivity, and

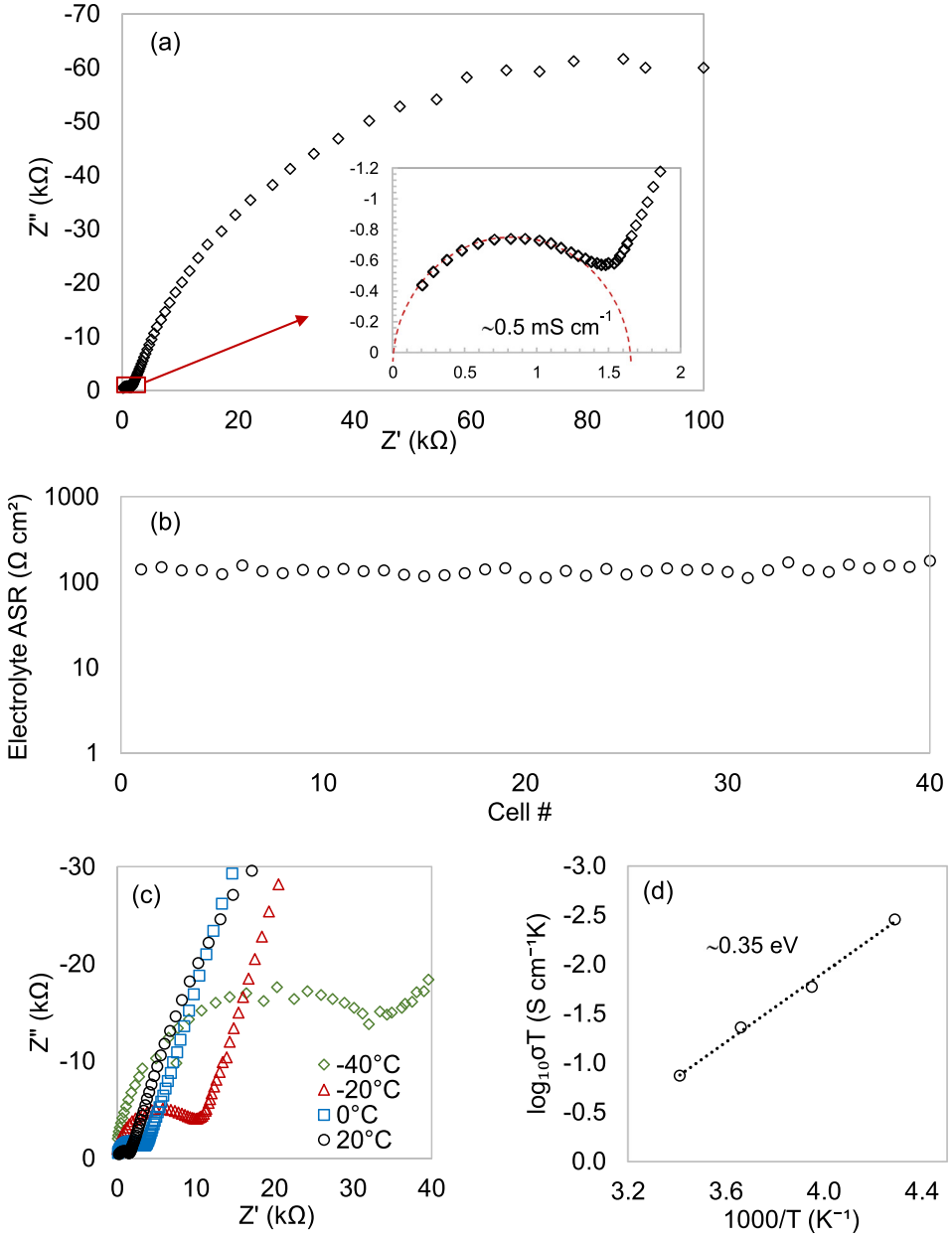

Fig. 4. (a) Typical impedance spectrum of flash sintered LLZO at room temperature with Li electrodes zoomed at high frequency, (b) LLZO ASR for 40 symmetrical cells prepared with the same process, (c) impedance spectra of flash sintered LLZO at 20, 0, −20, −40 °C, and (d) Arrhenius plot of the total conductivity of LLZO.

with a high degree of reproducibility can be made by the flash sintering process. However, care must be taken to optimize the flash parameters (the furnace temperature, the field and the current density limit) in order to obtain specimens which are of high relative density and have a uniform microstructure. The lithium-ion conductivity measured with impedance spectroscopy was 0.5 mS cm^{-1} at room temperature, and the activation energy was 0.35 eV, similar to the values reported in the literature with conventional or hot-pressing techniques.

While the scale-up of flash sintering for solid-state battery applications remains unresolved, the present technique can be useful to filter the influence of compositions and doping on the electrochemical properties of such compounds, in an expedient manner.

Acknowledgements

This research was supported by a project from ARPA-E award Number DE-AR0000777 under an agreement for Cooperative Research with the ARPA-E team led by Dr. Paul Albertus. We thank him and his team for invaluable discussions and inputs. We thank Prof. D. L. Williamson at the Colorado School of Mines for his advice and help with X-ray diffraction measurements.

References

[1] M. Cologna, B. Rashkova, R. Raj, J. Am. Ceram. Soc. 93 (11) (2010 Nov) 3556–3559.
[2] P. Dahl, I. Kaus, Z. Zhao, M. Johnsson, M. Nygren, K. Wiik, T. Grande, M.A. Einarsrud, Ceram. Int. 33 (8) (2007 Dec 1) 1603–1610.
[3] M. Yu, S. Grasso, R. Mckinnon, T. Saunders, M.J. Reece, Adv. Appl. Ceram. 116 (1) (2017 Jan 2) 24–60.
[4] R. Raj, J. Eur. Ceram. Soc. 32 (10) (2012 Aug 1) 2293–2301.
[5] R. Murugan, V. Thangadurai, W. Weppner, Angew. Chem. Int. Ed. 46 (41) (2007 Oct 15) 7778–7781.
[6] R. Sudo, Y. Nakata, K. Ishiguro, M. Matsui, A. Hirano, Y. Takeda, O. Yamamoto, N. Imanishi, Solid State Ionics 262 (2014 Sep 1) 151–154.
[7] S. Hu, Y.F. Li, R. Yang, Z. Yang, L. Wang, Ceram. Int. 44 (6) (2018 Apr 15) 6614–6618.
[8] H. Buschmann, J. Dölle, S. Berendts, A. Kuhn, et al., Phys. Chem. Chem. Phys. 13 (2011 Aug) 19378–19392.
[9] E. Rangasamy, J. Wolfenstine, J. Sakamoto, Solid State Ionics 206 (2012 Jan 5) 28–32.
[10] A. Sharafi, H.M. Meyer, J. Nanda, J. Wolfenstine, J. Sakamoto, J. Power Sources 302 (2016 Jan 20) 135–139.
[11] A. Sharafi, C.G. Haslam, R.D. Kerns, J. Wolfenstine, J. Sakamoto, J. Mater. Chem. A 5 (40) (2017) 21491–21504.
[12] I.N. David, T. Thompson, J. Wolfenstine, J.L. Allen, J. Sakamoto, J. Am. Ceram. Soc. 98 (4) (2015 Apr) 1209–1214.
[13] R. Raj, J. Am. Ceram. Soc. 65 (3) (1982 Mar) (C-46).
[14] J.S. Francis, R. Raj, J. Am. Ceram. Soc. 96 (9) (2013 Sep) 2754–2758.
[15] J. Tan, A. Tiwari, Electrochem. Solid-State Lett. 15 (3) (2011 Jan 1) A37–A39.
[16] J. Wolfenstine, H. Jo, Y.H. Cho, I.N. David, P. Askeland, E.D. Case, H. Kim, H. Choe, J. Sakamoto, Mater. Lett. 96 (2013 Apr 1) 117–120.
[17] G.R. Anstis, P. Chantikul, B.R. Lawn, D.B. Marshall, J. Am. Ceram. Soc. 64 (9) (1981 Sep) 533–538.
[18] J.E. Ni, E.D. Case, J.S. Sakamoto, E. Rangasamy, J.B. Wolfenstine, J. Mater. Sci. 47 (23) (2012 Dec 1) 7978–7985.
[19] J.F. Wu, E.Y. Chen, Y. Yu, L. Liu, Y. Wu, W.K. Pang, V.K. Peterson, X. Guo, ACS Appl. Mater. Interfaces 9 (2) (2017 Jan 5) 1542–1552.
[20] L. Cheng, E.J. Crumlin, W. Chen, R. Qiao, H. Hou, S.F. Lux, V. Zorba, R. Russo, R. Kostecki, Z. Liu, K. Persson, Phys. Chem. Chem. Phys. 16 (34) (2014) 18294–18300.
[21] C. Deviannapoorani, L. Dhivya, S. Ramakumar, R. Murugan, J. Power Sources 240 (2013 Oct 15) 18–25.
[22] J. Awaka, N. Kijima, H. Hayakawa, J. Akimoto, J. Solid State Chem. 182 (8) (2009 Aug 1) 2046–2052.